CrossMark

Excitation performance of fabricated PMN–BFO relaxor through electric field

S. N. Das[1] · S. K. Pradhan[1] · D. P. Kar[1] · S. Bhuyan[1] · R. N. P. Choudhary[1]

Abstract

The lead magnesium niobate (PMN; $PbMg_{1/3}Nb_{2/3}O_3$) and bismuth ferrite (BFO; $BiFeO_3$) electronic compound has been fabricated and its excitation through electric field has been experimentally investigated. The unveiled excellent material properties like frequency independent and temperature dependent high dielectric constant and low dielectric loss substantiate the relaxor behavior of the processed material. A parallel plate capacitor structure is designed in order to reveal the material's excitation through the generated internal electric field which has also been affirmed. The experimental results exhibit the dependence of excitation intensity on the material properties, driving frequency, relative position and generated electric field strength. The intensity of excitation attains its peak when the driving frequency is synchronized with the mechanical resonant frequency of the fabricated relaxor dielectric component.

1 Introduction

There has been rapid research growth in the development of functional dielectric ceramic electronic materials due to their wide usability as sensors, ultrasonic detector, resonators, filters, capacitors and actuators [1–6]. In order to enlighten as a budding contender, the ceramic materials necessitate excellent properties like high dielectric constant, low dielectric loss, broad-frequency dispersion, high electrostriction property, super voltage stability and thermally stable resonant frequency [7–14]. Providentially, the multiferroic materials in tandem with the lead magnesium niobate (PMN) relaxor has been considered as promising entrant due to their notable dielectric and physical properties [15–19]. They can be driven by the application of electric fields, magnetic fields, or strain between different structural/electronic phases. Therefore, there is a heave of research attention in the development of $PbMg_{1/3}Nb_{2/3}O_3$–$BiFeO_3$ polarized electronic component which is an exclusive multiferroic material having significant dielectric properties for potential device applications. In this letter, in view of its importance, this electronic material has been processed using high temperature solid state chemical reaction technique. The X-ray structural exploration, morphology, chemical concentration analysis, and dielectric characterizations including capacitive, conducting and relaxor behavior along with the dielectric dispersion and phase transition have been experimentally investigated. In order to ascertain the influence of electric field, the designed PMN–BFO component has been inserted between the electrodes of a parallel plate capacitor structured electric field generator. The electric field receptiveness props up the developed material as a competent entity for potential device applications.

2 Experimental procedure for material synthesis

The dense ceramic compound $0.5PbMg_{1/3}Nb_{2/3}O_3$–$0.5Bi_2FeO_3$ has been prepared by taking the analytical reagent (AR) grade (> 99.9% purity obtained from Loba Chemie) powder of PbO (lead oxide), MgO (magnesium oxide), Fe_2O_3 (iron oxide) and Nb_2O_5 (niobium oxide) in appropriate proportion (with 2% extra bismuth oxide) by using the conventional high temperature solid state reaction method [20]. Calcinations of the homogeneous solid solution is carried out in a high temperature furnace by increasing the temperatures in steps and holding at temperature 810 °C for a duration of 6 h. The calcined powder is examined through X-ray crystallography at room temperature for preliminary affirmation of perovskite solid solution $0.5PbMg_{1/3}Nb_{2/3}O_3$–$0.5Bi_2FeO_3$. Disk shape pallet

✉ S. Bhuyan
satyanarayanbhuyan@soa.ac.in

1   Siksha 'O' Anusandhan (Deemed to be University), Bhubaneswar 751030, India

of 12 mm diameter and 1 mm thickness are prepared by adding PVA binder for granulation through a uniaxial hydraulic press by applying a pressure of 25 MPa. These pallets are sintered at a temperature of 850 °C for 4 h and density of the samples obtained to be 94% (measured by Archimedes principle). These dense pallets are electroded in (001) direction through pure silver (Ag) paste for its electrical characterization by using a LCR meter (N4L PSM1735) over a wide range of frequency (1 kHz–1 MHz) and temperature (25–500 °C).

3 Results and analysis

Figure 1a illustrates X-ray diffraction (XRD) spectrum of calcinated $0.5PbMg_{1/3}Nb_{2/3}O_3$–$0.5Bi_2FeO_3$ at room temperature. The room temperature XRD pattern of calcined PMN–BFO powder sample is obtained through XRD technique (X-ray powder diffractometer), Rigaku Miniflex, Japan, $\lambda = 1.5404$ Å, Bragg angle θ ($20° \leq 2\theta \leq 70°$, at a scanning rate of 2°/min). As the location and intensity of all the distinct reflection peaks differs from the ingredients, it implies the formation of PMN–BFO compound. The standard computer program package POWD [21] has been used to calculate the structural parameters of the sample and indexing of all the reflections of the XRD pattern and compared with ICCD files. Using 2θ values of diffraction peaks, prominent peaks of the pattern have been indexed and refined using the least-squares sub-routine of the standard-computer program package POWD. With the help of best fit as well as the smallest difference among the experimental values and model parameters of inter-planar spacing of each reflection, orthorhombic crystal unit cell has been selected.
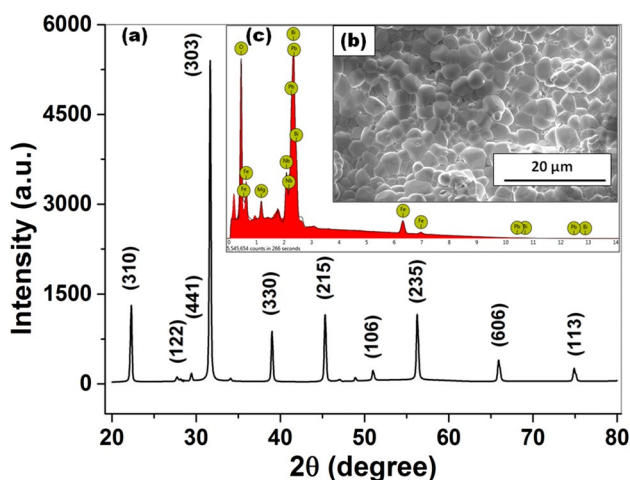
The surface morphology of PMN–BFO can be revealed from the scanning electron microscopic image of sintered pellets as shown in Fig. 1b. Grains of different dimensions and shapes (1.9–3.2 µm) have been distributed homogeneously over the surface with high density that can be noticed from the micrograph. The high temperature sintering of the sample has helped to get almost free from irregular shape of voids. Again the stoichiometric composition of the prepared sample is examined by EDS (energy dispersive X-ray spectroscopy) analysis as depicted in Fig. 1c, which is similar to its base compositions with no impurity content.

Figure 2 represents the dielectric constant and tangent loss dependency characteristics on a wide range of temperature (25–500 °C) as well as frequency (1 kHz–1 MHz). The temperature reliance of relative permittivity reveals the relaxor region (dielectric constant is temperature dependent and frequency independent) and magnetic transition region (dielectric constant is both temperature and frequency dependent). With the temperature rise, the relative permittivity ascends to a maximum (ε_{max}) value at the relaxor region, and there after remains constant in the frequency independent section which approximately ranges from 150 to 250 °C. After wards, another peak appears above 400 °C which may be due to the ferroelectric–paraelectric (FE–PE) or ferroelectric–ferroelectric (FE–FE) phase transition. Similarly at low frequency it has superior dielectric constant value which declines gradually with increase in frequency which is the general trend of dielectrics. This is due to the accumulation of charge carriers and defects due to the presence of multivalence cations at the inter face. From the plot, it is evident that the fabricated electronic material is a strong function of both temperature and frequency. The relaxor behavior of the compound can be substantiated from the following characteristics: (i) diffusive characteristic of frequency
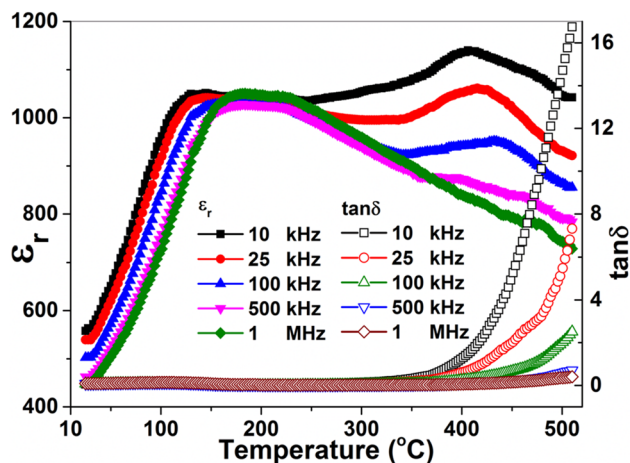

Fig. 1 (*a*) XRD spectrum of calcinated $0.5PbMg_{1/3}Nb_{2/3}O_3$–$0.5Bi_2FeO_3$ at room temperature; (*b*) SEM micrograph of PMN–BFO sintered pellets; (*c*) EDS spectra of different element of $0.5PbMg_{1/3}Nb_{2/3}O_3$–$0.5Bi_2FeO_3$

Fig. 2 Temperature dependence of dielectric constant and tangent loss at selected frequencies of $0.5PbMg_{1/3}Nb_{2/3}O_3$–$0.5Bi_2FeO_3$

reliance dielectric maxima, (ii) broadening of peak at higher frequencies, (iii) shifting of broadened toward higher temperature with frequency, (iv) frequency independency nature in-between relaxor region and magnetic transition region. These are may be due to the existence of polar nano regions (PNRs) in the processed material [22–24]. At higher frequency the role of PNR clusters starts vanishing validating the widened peak.

It can be elucidated from the tangent loss spectrum that at low temperature, the losses are minimum, and it increases sharply at higher temperatures which may be originated from multiple oxidation state of elements (Pb/Nb/Fe) that inter change spontaneously causing the oxygen vacancies to retain the local electrical neutrality and responsible for thermally triggered hopping conduction. At high frequency the loss factor decreases that may be due to the inability of charge carriers to accumulate at the interface within a very short span of time.

The cole–cole plot (Nyquist plot, as illustrated in Fig. 3) gives the idea about the relaxation process, conductive nature as well as the grain and grain boundary effect. This plot signifies a straight line at lower temperature parallel to y-axis representing poor conducting property of the samples. Gradually as temperature increases, the lines bends towards the x-axis confirming the rise in conducting property of the samples at higher temperature. At a temperature above 400 °C the semicircular arc formation affinity is observed, and the semicircle maps out the bulk property (grain property). The experimentally observed impedance data's are fitted with a circuit model (Z-win software) that comprises a parallel connection of C_b and R_b which is further series connected with parallel combination of R_{gb}, C_{gb} and a constant phase element (where C_b = bulk capacitance, R_b = bulk resistance, R_{gb} = grain resistance and C_{gb} = grain capacitance, respectively). The calculated fitting parameters

are given in Table 1 which provides the grain and grain boundary contribution to the total conductivity/resistivity of the material. The non occurrence of perfect semicircular arc reveals the non Debye-type relaxation [25–28]. The negative temperature coefficient of resistance as well as semiconducting nature of the samples has been exposed.

4 Experimental set up and excitation performance

To investigate the excitation of the prepared PMN–BFO electronic component through electric field, an experimental setup has been designed, as illustrated in Fig. 4. In the experimental design, for the generation of an ac electric field, an ac voltage source with tunable frequency is connected to the two copper plate-shaped live and ground electrodes mounted on a plastic board with a changeable separation which forms a parallel plate capacitor structure. The parallel plate capacitor structure is intended to generate uniform ac electric field.

Table 1 Fitting parameters of Bulk and grain boundary resistance as well as capacitance of impedance parameters of the compound $0.5PbMg_{1/3}Nb_{2/3}O_3$–$0.5Bi_2FeO_3$

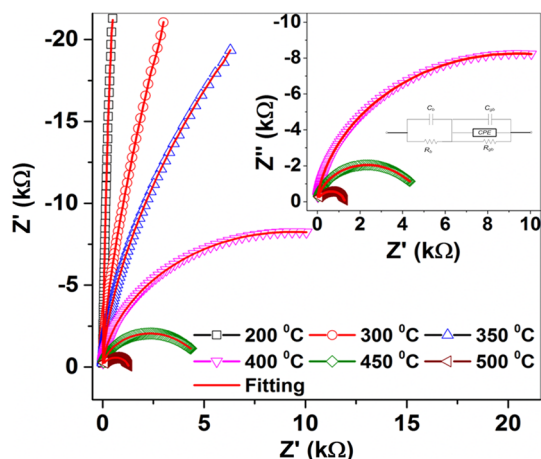| Temperature (°C)	R_b (Ω)	C_b (F)	R_{gb} (Ω)	CPE	C_{gb} (F)
200	4.23E+01	1.46E−10	1.32E+15	5.14E−07	5.21E−08
300	3.96E+00	2.42E−09	3.76E+10	3.26E−07	2.58E−08
350	2.35E+01	3.11E−09	2.79E+07	7.44E−07	3.21E−09
400	3.87E+00	5.15E−08	1.55E+04	2.39E−08	8.52E−09
450	2.02E+01	6.13E−08	3.77E+03	3.32E−08	2.78E−10
500	1.92E+01	1.54E−07	6.23E+02	6.46E−07	8.55E−10

Fig. 3 Nyquist plot of $0.5PbMg_{1/3}Nb_{2/3}O_3$–$0.5Bi_2FeO_3$ with equivalent circuit model
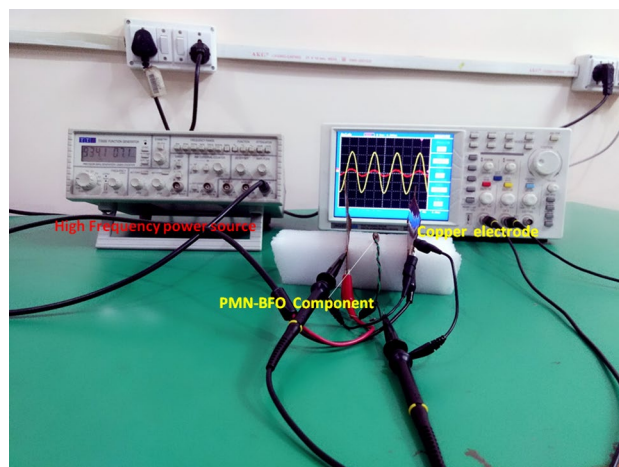

Fig. 4 Experimental setup to drive PMN–BFO dielectric component by the application electric field generated by a parallel plate capacitor structure

The fabricated polarized dielectric component (PMN–BFO) is inserted into the physical gap between the live and ground electrodes of capacitor structure, and equidistantly placed parallel to both the two electrodes. To measure the voltage developed across the dielectric component due to the excitation, two lead wires are soldered onto the surface electrodes of the component.

When the polarized PMN–BFO dielectric component is placed in an externally electric field, the component gets strained or deformed structurally as result of the penetration of electric field. Consequently, a voltage is observed across the surface electrodes of the PMN–BFO dielectric component. If the generated electric field frequency synchronizes with mechanical resonant frequency of the dielectric

Fig. 5 Excitation mechanism of dielectric component through electric field

component, a mechanical resonance can be excited. This mechanical resonance generates a relatively large voltage across the surface electrodes of the component. This can also be explained by using the Gauss's law. If D is the electric displacement vector, ε is the permittivity and $\widetilde{E}$ is the average electric field on the surface of the component, then charge on the surface of dielectric component (as depicted in Fig. 5) is given by

$$\sigma_S = D - \varepsilon \widetilde{E} \tag{1}$$

The frequency characteristic of the voltage developed across the surface of dielectric component (measured open circuit voltage) is depicted in Fig. 6a. It is realized that when the electric field generated by the parallel plate capacitor structure penetrates to the polarized dielectric component, the component gets excited. Consequently, a voltage is developed across the surface electrode of the excited component that resulted from the electric field. It has also been seen that when the operating frequency is matched with the mechanical resonance frequency (observed as 882 kHz) of the component, the voltage across the dielectric component is found to be maximum due to the mechanical resonance of the component. The experimental result affirms the influence of electric field on the prepared $0.5PbMg_{1/3}Nb_{2/3}O_3–0.5Bi_2FeO_3$ electronic component. To determine the effect of electric field with the physical separation gap, the experiment has been carried out by varying the physical separation gap between the live and ground electrodes of parallel plate structure keeping the dielectric component fixed along the
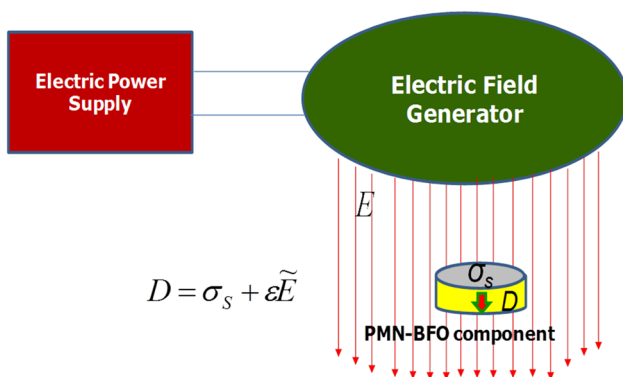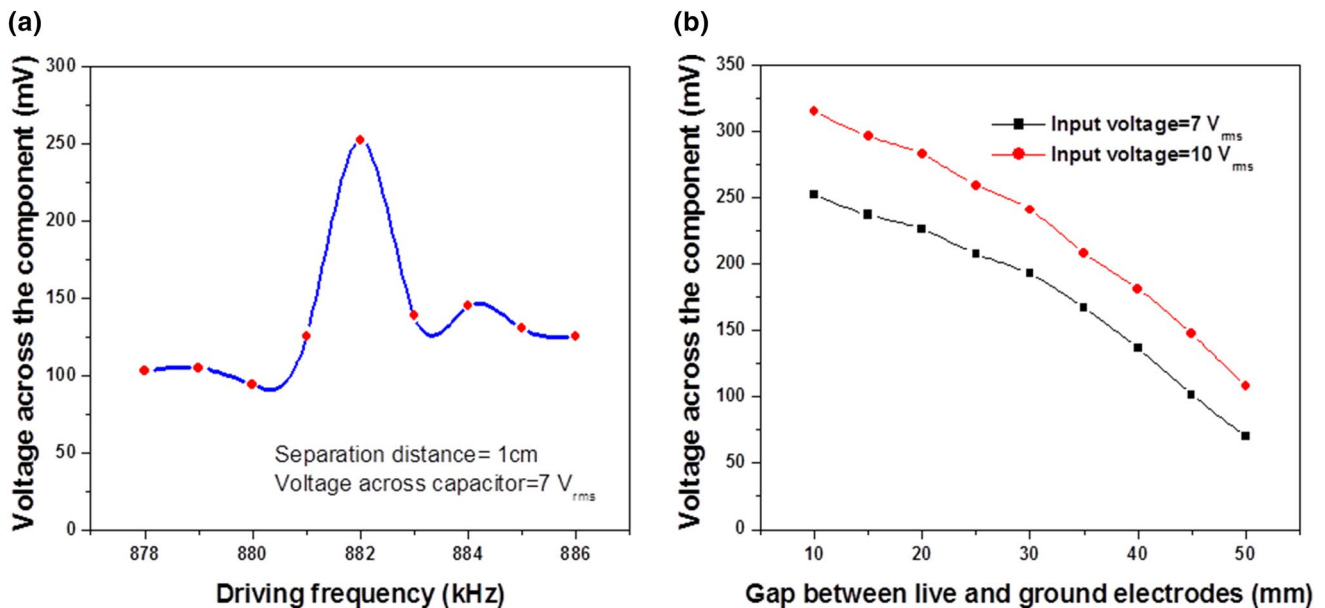

Fig. 6 **a** Frequency characteristic of the voltage developed across the surface of dielectric component; **b** dependence of the maximum excitation voltage across the dielectric component on the input voltage and gap thickness between the two parallel electrodes

central axis. The observed results are illustrated in Fig. 6b. It is observed that the voltage across the dielectric component declines with the increase in physical separation gap which may be due to the decrease in electric field intensity. This finding well agrees with the concept of electric field that the electric field intensity is directly proportional to the input voltage and inversely proportional with the gap thickness between the electrodes of a parallel plate capacitor.

5 Conclusion

The electronic compound $[0.5PbMg_{1/3}Nb_{2/3}O_3–0.5Bi_2FeO_3]$ has been fabricated through solid state chemical reaction technique. The formation of the desired sample material is confirmed with a rhombohedral structure using room temperature XRD analysis, the uniform grain distribution is predicted from the micrograph and its composition has been corroborated from the EDS analysis. The investigated morphological, structural, dielectric, capacitive and conducting characteristics reveals the relaxor behavior of the prepared material. The excitation of the prepared material has been practically examined through the electric field generated by a designed parallel plate capacitor structure. The developed electronic component may have the propensity as an actuator for potential applications in miniature driving mechanisms, precise positioning and particle manipulations.

References

1. Y. Zhang, Q. Chi, L. Liu, C. Zhang, C. Chen, X. Wang, Q.Q. Lei, Appl. Phys. Lett. **5**, 076109 (2017)
2. M. Song, I. Iorsh, P. Kapitanova, E. Nenasheva, P. Belov, Appl. Phys. Lett. **108**, 023902 (2016)
3. M.S. Awan, A.S. Bhatti, J. Mater. Eng. Perform. **20**, 283 (2011)
4. D.F. Wang, X. Lou, A. Bao, X. Yang, J. Zhao, Appl. Phys. Lett. **111**, 083502 (2017)
5. S.N. Das, S.K. Pradhan, S. Bhuyan, S. Sahoo, R.N.P. Choudhary, M.N. Goswami, J. Electron. Mater. **47**, 843 (2017)
6. X. Zhang, L. Yang, H. Ji, J. Qui, J. Mater. Sci.: Mater. Electron. **29**, 3602 (2018)
7. A. Tripathy, S. Pramanik, A. Manna, S. Bhuyan, N.F.A. Shah, Z. Radzi, N.A.A. Osman, Sensors **16**, 1135 (2016)
8. S.K. Pradhan, S.N. Das, S. Halder, S. Bhuyan, R.N.P. Choudhary, J. Electron. Mater. **28**, 9627 (2017)
9. J.D. Bobic, R.M. Katiliute, M. Ivanov, M.M. Vijatovic´, N.I. Petrovic´, A.S. Ilic´, J. Dzˇunuzovic´, B.D. Banys, Stojanovic´, J. Mater. Sci.: Mater. Electron. **27**, 2448 (2016)
10. S. Halder, K. Parida, S.N. Das, S. Bhuyan, R.N.P. Choudhary, J. Mater. Sci.: Mater. Electron. **28**, 15928 (2017)
11. W.B. Luo, L.G. Chen, J. Meng, Y. Shuai, C.G. Wu, X.Y. Sun, L. andW, Zhang, J. Mater. Sci.: Mater. Electron. **29**, 271 (2018)
12. W. Wang, S. Wang, Y. Zhang., X. Zhao. H. Luo, J. Electron. Mater. **40**, 11 (2011)
13. W. Eerenstein, N.D. Mathur, J.F. Scott, Nature (London) **442**, 759 (2006)
14. R. Wen, L. Zhou, L. Luo, N. Jiang, Q. Zheng, J. Liao, C. Xu, D. Lin, J. Mater. Sci.: Mater. Electron. **26**, 8341 (2015)
15. G. Singh, V.S. Tiwari, J. Appl. Phys. **101**, 014115 (2007)
16. S.N. Das, S.K. Pradhan, S. Bhuyan, R.N.P. Choudhary, J. Mater. Sci.: Mater. Electron. **28**, 18913 (2017)
17. S.N. Das, S. Pradhan, S. Bhuyan, R.N.P. Choudhary, P. Das, J. Electron. Mater. **46**, 1637 (2017)
18. M.M. Kumar, V.R. Palkar, K. Srinivas, S.V. Suryanarayana, Appl. Phys. Lett. **76**, 2764 (2000)
19. P.K. Bajpai, M. Pastor, K.N. Singh, J. Electron. Mater. **43**, 1403 (2014)
20. S.K. Pradhan, S.N. Das, S. Bhuyan, C. Behera, R. Padhee, R.N.P. Choudhary, Appl. Phys. A **122**, 604 (2016)
21. E. Wu, J. Appl. Cryst. **22**, 506 (1989)
22. A. Tripathy, S.N. Das, S.K. Pradhan, S. Bhuyan, R.N.P. Choudhary, J. Mater. Sci.: Mater. Electron. **29**, 4770 (2018)
23. V.R. Palkar, J. John, R. Pinto, Appl. Phys. Lett. **80**, 1628 (2002)
24. Y.P. Wang, L. Zhou, M.F. Zhang, X.Y. Chen, J.M. Liu, Z.G. Liu, Appl. Phys. Lett. **84**, 1731 (2004)
25. K.K. Mishra, A.T. Satya, A. Bharathi, V. Sivasubramanian, V.R.K. Murthy, A.K. Arora, J. Appl. Phys. **110**, 123529 (2011)
26. S.N. Das, A. Pattanaik, S. Kadambini, S. Pradhan, S. Bhuyan, R.N.P. Choudhary, J. Mater. Sci.: Mater. Electron. **27**, 10099 (2016)
27. S.K. Pradhan, S.N. Das, S. Bhuyan, C. Behera, R.N.P. Choudhary, J. Mater. Sci.: Mater. Electron. **28**, 1186 (2017)
28. S. Halder, K. Parida, S.N. Das, S. Bhuyan, R.N.P. Choudhary, Phys. Lett. A **382**, 716 (2018)